Journal of The Electrochemical Society, **151** (8) A1134-A1140 (2004)
0013-4651/2004/151(8)/A1134/7/$7.00 © The Electrochemical Society, Inc.

Combining *Ab Initio* Computation with Experiments for Designing New Electrode Materials for Advanced Lithium Batteries: $LiNi_{1/3}Fe_{1/6}Co_{1/6}Mn_{1/3}O_2$

Ying S. Meng,[a] Yei Wei Wu,[b] Bing Joe Hwang,[b,d,*] Yi Li,[a,c] and Gerbrand Ceder[a,d,*]

[a]*Singapore-MIT Alliance, Advanced Materials for Micro- and Nano-Systems Programme, Singapore 117576*
[b]*Department of Chemical Engineering, National Taiwan University of Science and Technology, Taipei, Taiwan 106*
[c]*Department of Materials Science, National University of Singapore, Lower Kent Ridge, Singapore 119260*
[d]*Department of Materials Science and Engineering, Massachusetts Institute of Technology, Cambridge, Massachusetts 02139, USA*

An initial search with density functional theory to sort through potential cathode materials based on their Li intercalation potentials and electronic structures was carried on $LiNi_{1/3}TM1_{1/3}TM2_{1/3}O_2$ systems, where TM1 is a 3+ transition metal (Co^{3+}, Al^{3+}, Fe^{3+} etc.) and TM2 is a 4+ transition metal (Ti^{4+}, Zr^{4+}, Mn^{4+} etc.). Fe substitution is found to be advantageous because among the compounds investigated it shows the lowest voltage at the last stage of the charge. $LiNi_{1/3}Fe_{1/6}Co_{1/6}Mn_{1/3}O_2$ was synthesized by a sol-gel method and used to confirm that Fe substitution leads to a lower potential at the end of charge. Both X-ray photoelectron spectroscopy and first principles electronic structure computations indicate that Ni and Fe are simultaneously oxidized in this material. Computations further indicate that Co will only be oxidized at the very end of charge. The $LiNi_{1/3}Fe_{1/6}Co_{1/6}Mn_{1/3}O_2$ compound synthesized at 750°C shows reversible capacity of 150 mAh/g with reasonably good capacity retention.
 [DOI: 10.1149/1.1765032]

Manuscript submitted November 3, 2003; revised manuscript received January 26, 2004. Available electronically June 17, 2004.

Lithium nickel manganese oxide and their derivatives are considered promising candidates for future lithium ion batteries.[1-3] In these compounds, nickel can exchange two electrons so that manganese can remain at a 4+ oxidation state during the charge-discharge cycle without any loss of theoretical capacity (about 280 mAh/g) and without the instabilities associated with more reduced states of Mn.[4] Recently, $LiNi_{1/3}Co_{1/3}Mn_{1/3}O_2$ has been shown to have very good electrochemical properties. Ohzuku *et al.* reported that $LiNi_{1/3}Co_{1/3}Mn_{1/3}O_2$ has 200 mAh/g in the voltage range of 2.5-4.6 V with negligible capacity loss up to 30 cycles.[5] Hwang *et al.* obtained reversible capacity of 188 mAh/g in the potential window of 3 to 4.5 V.[6] Shaju *et al.* inferred from cyclic voltammetry (CV) results that the redox processes at 3.8 and 4.6 V correspond to the Ni^{2+}/Ni^{4+} and Co^{3+}/Co^{4+} couples, respectively,[7] though the capacity from the latter redox pair is very small in this potential window. First principles calculation confirmed that Co^{3+} is only oxidized to Co^{4+} at rather high voltage in this material.[6] While first principles methods are not accurate enough to exactly predict voltages, the computational results in Ref. 6 indicate that complete oxidation of Co^{3+} to Co^{4+} may require potentials near 5 V in this system. An obvious way to increase practical capacity is therefore to partially substitute Co or Mn by other transition metals, which either bring down the redox potential of Co, or introduce another redox couple in a lower voltage range than Co^{3+}/Co^{4+}.

$LiNi_{1/3}Co_{1/3}Mn_{1/3}O_2$ illustrates the recent trend towards multicomponent transition metal oxides, which creates a large number of possible compositional choices. The materials development including synthesis, processing, characterization, and optimization can be more efficient and cost effective if we can do a certain amount of property prediction and optimization during the design stage. We therefore performed an initial search with density functional theory (DFT) to evaluate the Li (de)intercalation voltage of potential cathode materials. Through first principles computation methods, we identified partial substitution of Co by Fe in $LiNi_{1/3}Co_{1/3}Mn_{1/3}O_2$ as a way of lowering the lithium (de)intercalation potential at the end of charge. Structural energies and calculated mixing enthalpies were used to guide the synthesis conditions and help interpret experimental results. In this paper, we present how a new potential cathode material $LiNi_{1/3}Fe_{1/6}Co_{1/6}Mn_{1/3}O_2$ is designed, synthesized and characterized by an approach integrating *ab initio* computation and experiments.

Methodology

Computational.—It has been amply demonstrated that reasonable lithium intercalation potentials and geometrical information can be obtained with first principles methods.[8-10] To describe the $Li_xNi_{1/3}Fe_{1/6}Co_{1/6}Mn_{1/3}O_2$ system, supercells with six formula units were used. As it is typical in solid state computations periodic boundaries are used, so that one effectively models a system with Ni, Fe Co, and Mn long-range ordered (Fig. 1.) The effect of disorder, present in a real system, would likely smooth the voltage curve from what is achieved computationally.

All energies, intercalation potentials, geometries, and electronic structure of materials in this paper were obtained using first-principles quantum mechanics in the generalized gradient approximation (GGA) to DFT, as implemented in the vienna *ab initio* simulation package (VASP). Ultrasoft pseudo-potentials are applied to represent the nuclei and core electrons and all structures are fully relaxed with respect to internal and external cell parameters. The wave functions are expanded in plane waves with energy below 405 eV. Brillouin zone integration of the band structure is performed with a $6 \times 3 \times 4$ mesh. All calculations are performed with spin polarization, previously demonstrated to be crucial in manganese oxides.[11] Both ferromagnetic and anti-ferromagnetic spin polarization was taken into consideration. For each Li concentration x, antiferromagnetic coupling among Ni, Mn, and Fe gives a lower energy than ferromagnetic coupling.

Partial states of delithiation were investigated at $x = 5/6$, 2/3, 1/2, 1/3, and 1/6. The number of possible arrangements for Li and vacant sites in the supercell are 1, 6, 15, 20, 15, 6, and 1 for $x = 1$, 5/6, 2/3, 1/2, 1/3, 1/6, and 0, respectively. All possible arrangements have been calculated.

Experimental.—Motivated by the first principles results, $LiNi_{1/3}Fe_{1/6}Co_{1/6}Mn_{1/3}O_2$ was synthesized by a sol-gel method using citric acid as a chelating agent. A stoichiometric amount of lithium acetate ($Li(CH_3COO)\cdot 2H_2O$), nickel acetate ($Ni(CH_3COO)_2\cdot 4H_2O$), cobalt nitrate ($Co(NO_3)_2\cdot 6H_2O$), iron nitrate ($Fe(NO_3)_3\cdot 9H_2O$) and manganese acetate

* Electrochemical Society Active Member.

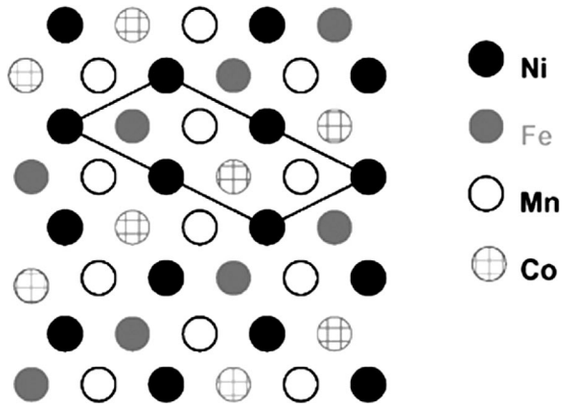

Figure 1. Ni, Fe, Co Mn ordering in the supercell of $Li(Ni_{1/3}Fe_{1/6}Co_{1/6}Mn_{1/3})O_2$.

$(Mn(CH_3COO)_2 \cdot 4H_2O)$ were dissolved in distilled water and well mixed with aqueous solution of citric acid. The solution was stirred at 60-70°C for 5-6 h to obtain a clear viscous gel. The gel was dried in vacuum oven at 120°C for 24 h. The material was precalcined in two stages: at 350°C for 5 h and 450°C for 4 h, and then ground before calcining at high temperature (750-900°C) at a heating rate of about 2°C/min. The powders were slowly cooled to room temperature in oxygen.

Powder X-ray diffraction (XRD) data were collected on a Rigaku diffractometer with Cu Kα1 radiation (λ = 1.5406 Å), operating at 300 kV and 60 mA. To minimize the preferred orientation effect, typical in layered lithium intercalation compounds, Vaseline is mixed with sample powders to randomize the orientation of the particles. Grain morphology and particle size of $LiNi_{1/3}Fe_{1/6}Co_{1/6}Mn_{1/3}O_2$ compounds were examined by scanning electron microscopy using a JEOL FEG-6320.

Information of nickel, cobalt, iron and manganese oxidation states in pristine and electrochemically-charged samples were obtained from X-ray photoelectron spectroscopy (XPS). Binding energies were charge-corrected using the C_{1s} peak (285 eV).

$LiNi_{1/3}Fe_{1/6}Co_{1/6}Mn_{1/3}O_2$ electrodes were fabricated by mixing 85:1.5:3.5:10 (w/w) ratio of active material, SS carbon black, KS-6 carbon and polyvinylidene fluoride (PVDF), respectively, using N-Methyl-pyrrolidone (NMP) as the solvent. The resulting slurry was cast onto an aluminum current collector, dried under vacuum oven for 4 h and put into an argon filled glove box for conditioning overnight. The electrode foils were roller-pressed to a uniform thickness of 100 μm and then cut into disks of 10 mm diam.

Electrochemical measurements were made using coin-type cells comprising Li metal counter electrode with a 1 M solution of $LiPF_6$ in EC/DMC (1:1 v/v, Merck LP30) as the electrolyte. The cells were assembled in the argon filled glove box where both moisture and oxygen levels are less than 1 ppm. The cells were charged and discharged using a Maccor battery tester at a C/10 rate (based on theoretical capacity of 281 mAh/g) over a potential range between 3.0 to 4.5 V.

Results and Discussion

First principles study of Co/Mn substitution.—An initial search on $LiNi_{1/3}TM1_{1/3}TM2_{1/3}O_2$ where TM1 is a 3+ transition metal (Co^{3+}, Al^{3+}, Fe^{3+} etc) and TM2 is a 4+ transition metal (Ti^{4+}, Zr^{4+}, Mn^{4+} etc.) was carried out. Figure 2 shows the potential of some of the substituted compounds as average voltages over intervals of 1/3 Li composition. The stepwise nature of the curves is therefore artificial and due to the averaging of the potential over the specific composition interval.

Substitution of Mn by either Ti or Zr clearly increases the potential and is therefore not suitable to reduce the potential at the

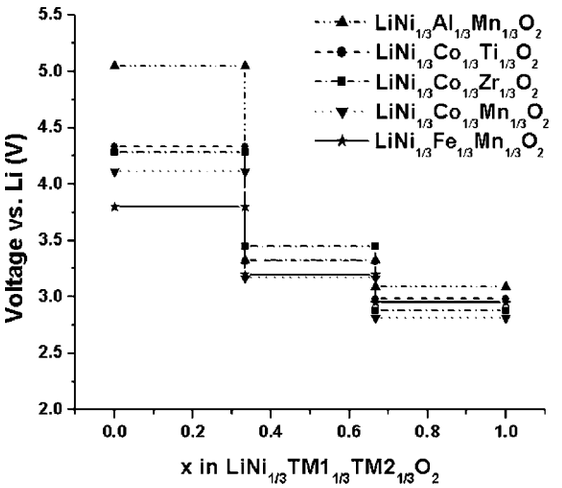

Figure 2. Calculated voltage curves for $LiNi_{1/3}TM1_{1/3}TM2_{1/3}O_2$ where TM1 = Al^{3+}, Co^{3+}, or Fe^{3+} and TM2 = Mn^{4+}, Ti^{4+}, or Zr^{4+}.

end of charge. In agreement with previous work on Al-doping,[10] substitution of Co by Al increases the potential. As it can not be oxidized beyond 3+, Al doping also reduces the capacity at the end of charge. Of all the compositional modifications investigated, Fe substitution of Co seems to be advantageous because it lowers the voltage profile at the last stage of the charge, compared to $LiNi_{1/3}Co_{1/3}Mn_{1/3}O_2$. Hence, the specific capacity of $LiNi_{1/3}Fe_{1/3}Mn_{1/3}O_2$ could be higher in the potential window of 3.0-4.5 V.

It is well known that due to the similar ion size of Fe^{3+} and Li^+, the Fe can partially occupy the Li-layer.[12-14] In addition, unlike $LiCoO_2$ and $LiNiO_2$, the $LiFeO_2$ ground-state structure is not layered, but a structure with symmetry $I4_1/amd$.[15] According to our preliminary mixing enthalpy calculations using the equation below, the relative formation energy of $LiNi_{1/3}Fe_{1/3}Mn_{1/3}O_2$ with respect to $LiNi_{1/2}Mn_{1/2}O_2$ and $LiFeO_2$ is approximately zero, indicating that only a weak entropic driving force for mixing might exist in a compound where Co is fully substituted by Fe

$$\langle \Delta E_{mix} = E_{LiNi_{1/3}Fe_xCo_{1/3-x}Mn_{1/3}O_2} - [2/3E_{LiNi_{1/2}Mn_{1/2}O_2} + zE_{LiFeO_2} + (1/3 - z)E_{LiCoO_2}] \rangle \quad [1]$$

Therefore, we chose to substitute Co only partially by Fe and targeted the nominal composition $LiNi_{1/3}Fe_{1/6}Co_{1/6}Mn_{1/3}O_2$ to obtain pure single-phase layered material.

Synthesis and characterization of as-prepared material.—The structure of the $LiNi_{1/3}Fe_{1/6}Co_{1/6}Mn_{1/3}O_2$ powders synthesized by sintering at 750, 800, and 850°C for 16 h were characterized using XRD (Cu Kα radiation), as shown in Fig. 3. XRD spectra show that all as-prepared samples have the α-$NaFeO_2$ type layered structure with space group R3-m. The two small peaks between 20 and 25° in 2θ are from Vaseline added to the sample. The region around the (104) reflection in the XRD spectra is shown in Fig. 3b. For powders synthesized at 750°C the (104) peak is broadened, indicating a small grain size, which was further confirmed by scanning electron microscopy (SEM) (Fig. 4a). For powders synthesized at 850°C an extra peak right beside the (104) peak (see Fig. 3b) starts to evolve. We suspect that this peak is related to the formation of a cation-disordered rock-salt structure. The clear splitting of the reflections assigned to the Miller indices (006, 102) and (108, 110) in the XRD spectrum of the 750 and 800°C sample indicates a well-layered structure.

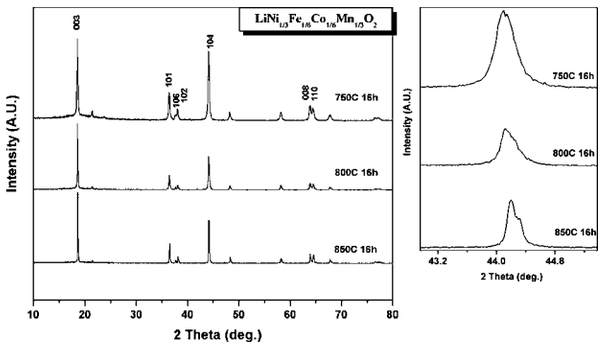

Figure 3. (a) XRD spectra of $LiNi_{1/3}Fe_{1/6}Co_{1/6}Mn_{1/3}O_2$ synthesized at 750, 800, and 850°C (b) Details of (104) peak in the XRD spectra of $LiNi_{1/3}Fe_{1/6}Co_{1/6}Mn_{1/3}O_2$ synthesized at 750, 800, and 850°C.

The lattice parameters a and c, determined from the sample synthesized at 750°C, are 2.8854 and 14.3221 Å, respectively. The calculated lattice parameters are 2.9138 and 14.3690 Å, which are slightly larger than those measured, as is often the case for computations in the generalized gradient approximation. In $LiNi_{1/3}Co_{1/3}Mn_{1/3}O_2$ synthesized at 900°C by the same sol-gel method, a and c are 2.864 and 14.247 Å, respectively.[6] The larger a and c lattice parameters of $LiNi_{1/3}Fe_{1/6}Co_{1/6}Mn_{1/3}O_2$ can be explained by the larger ion size of Fe^{III} as compared to Co^{III}.

A comparison of SEM micrographs obtained for $LiNi_{1/3}Fe_{1/6}Co_{1/6}Mn_{1/3}O_2$ synthesized at 750, 800, and 850°C is shown in Fig. 4. All samples have a uniform grain size and faceted grain morphology. The grains grow from 40-50 nm at 750°C to 300-500 nm at 850°C.

Intercalation potential.—Average voltage profiles for $Li_xNi_{1/3}Fe_{1/6}Co_{1/6}Mn_{1/3}O_2$ ($0 \leqslant x \leqslant 1$) were computed from the lowest energy lithium-vacancy arrangements in the six-formula supercell as function of lithium compositions. The calculated potentials are typically lower than experimental values, as is usuually the case in standard first principles energy methods.[4,16] The calculated intercalation voltage of $Li_xNi_{1/3}Fe_{1/6}Co_{1/6}Mn_{1/3}O_2$ is compared to that of $Li_xNi_{1/3}Co_{1/3}Mn_{1/3}O_2$ in Fig. 5. In the range $1/3 \leqslant x \leqslant 1$, a calculated average voltage of 3.0-3.1 V is obtained for $Li_xNi_{1/3}Fe_{1/6}Co_{1/6}Mn_{1/3}O_2$. The potential increases significantly to 3.8-3.9 V in the range $0 \leqslant x \leqslant 1/3$. Compared to $Li_xNi_{1/3}Co_{1/3}Mn_{1/3}O_2$,[6] (shown by the solid line in Fig. 5) the substitution of Fe with Co increases the average voltage slightly for $1/2 \leqslant x \leqslant 1$. Most importantly, in the Fe substituted compound, the calculated voltage at the end of charge ($0 \leqslant x \leqslant 1/3$) is much lower than that of $Li_xNi_{1/3}Co_{1/3}Mn_{1/3}O_2$. These results indicate that Fe substitution of Co in $LiNi_{1/3}Fe_zCo_{1/3-z}Mn_{1/3}O_2$ may flatten the voltage curve and increase the experimentally attainable capacity by lowering the potential near the end of charge.

Electrochemical characterization.—Electrodes of $LiNi_{1/3}Fe_{1/6}Co_{1/6}Mn_{1/3}O_2$ synthesized at 750, 800, and 850°C were cycled at a rate of C/10 (based on 281 mAh/g total capacity) between 3.0 and 4.5 V. The first charge and discharge curves for each sample are shown in Fig. 6. Qualitatively, the potential curves are very similar, exhibiting a relatively flat potential on charging in the range of 3.7 to 3.9 V, and then a relatively steeply sloping curve on discharge. The compound synthesized at 750°C shows smaller polarization which could be related to its smaller grain size. There is a significant amount of irreversible capacity after the first charge for all three samples. As the synthesis temperature increases from 750, 800, to 850°C, the first charge capacity decreases from 220 to 200-187 mAh/g, the first discharge capacity changes from 150 to 139-134 mAh/g. The capacity retention up to 30 cycles is reasonably good for all samples, as demonstrated in Fig. 7. The reason for the large first-cycle irreversible capacity is currently being investigated. A preliminary study shows that the first cycle reversible capacity can be increased by 20% with surface treatment of the synthesized powders.

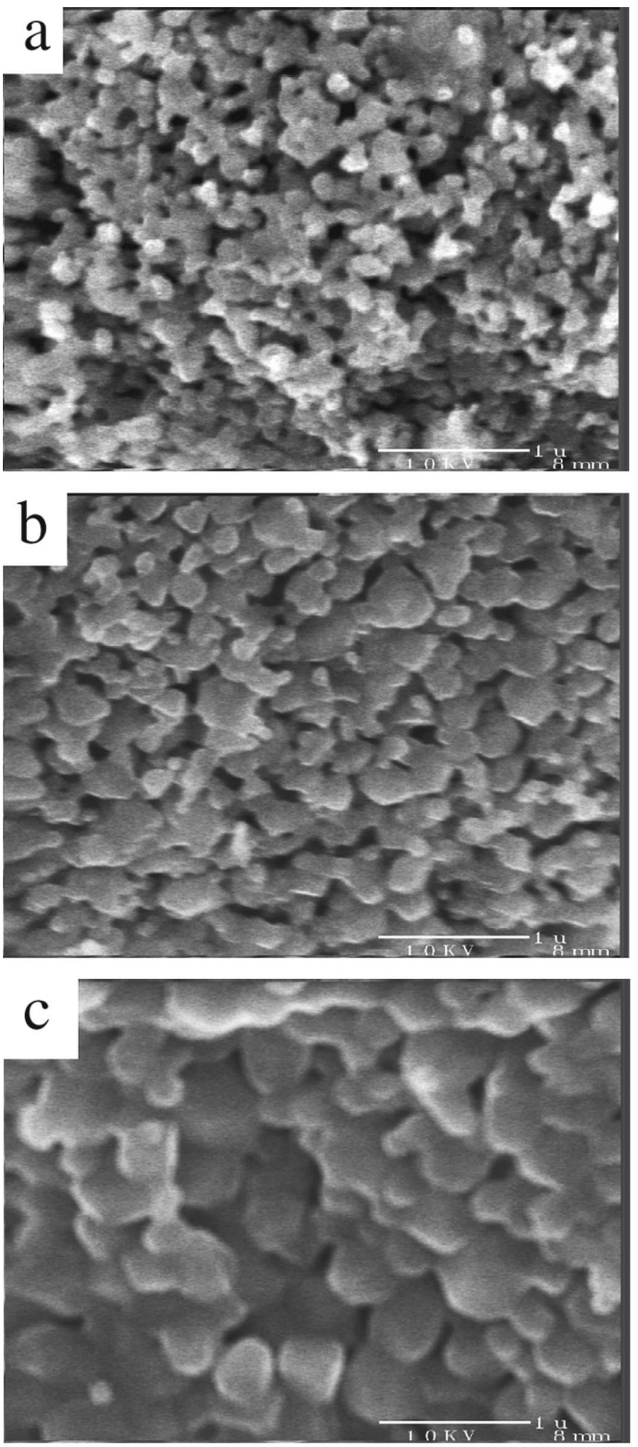

Figure 4. SEM images of as-prepared $LiNi_{1/3}Fe_{1/6}Co_{1/6}Mn_{1/3}O_2$ materials synthesized at (a) 750, (b) 800, and (c) 850°C.

The delithiation potential of the material synthesized at 750°C is plotted together with the calculated potential curve. The potential difference between the calculated and experimental data is suggested to be 0.7-0.8 V.[16] The correction of 0.9 V in this case was

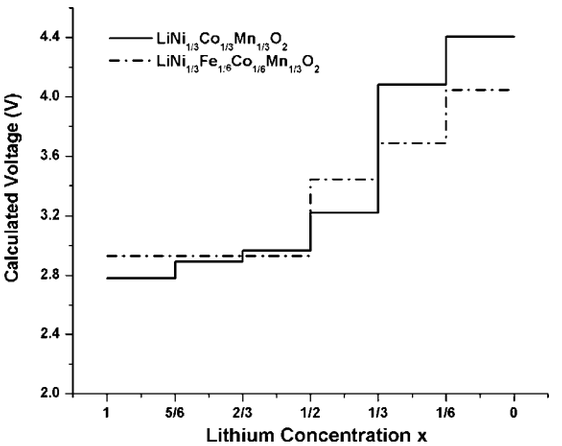

Figure 5. Comparison of calculated average voltage curves of $Li_xNi_{1/3}Co_{1/3}Mn_{1/3}O_2$ and $Li_xNi_{1/3}Fe_{1/6}Co_{1/6}Mn_{1/3}O_2$.

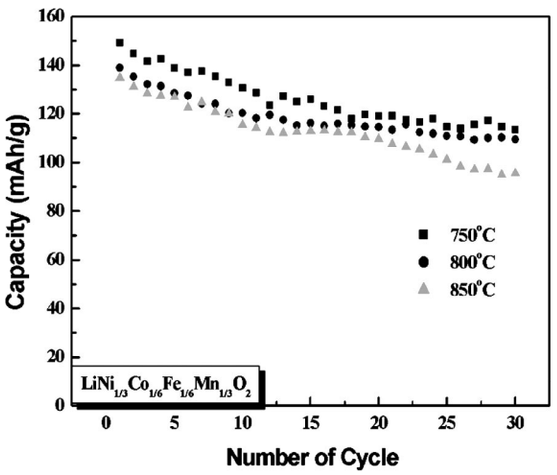

Figure 7. Charge and discharge capacity *vs.* cycle number curves of the $LiNi_{1/3}Fe_{1/6}Co_{1/6}Mn_{1/3}O_2$ materials synthesized at 750, 800, and 850°C for 16 h.

added to the calculated potential to display a result that can be compared directly with the experimental values, as shown in Fig. 8. The experimental charge-discharge curve matches the calculated one well in the range of $1/3 \leqslant x \leqslant 1$. The practical specific capacity of this material will likely be more than 250 mAh/g if the cell is charged to approximately 4.8 V, according to the computational prediction.

Electronic change during charge-discharge.—To understand the electronic changes in $LiNi_{1/3}Fe_{1/6}Co_{1/6}Mn_{1/3}O_2$ when lithium is removed, the spin polarized density of states (DOS) at different lithium concentrations is shown in Fig. 9. Because the transition metal ions occupy the octahedral sites in the sublattices of oxygen ions, 3d bands of transition metal ions split into t_{2g} and e_g bands. The calculated DOS, projected onto the orbitals of each transition metal are shown in Fig. 9.

For all lithium compositions, the Mn-t_{2g} and Mn-e_g bands are, respectively, half filled and empty in $Li_xNi_{1/3}Fe_{1/6}Co_{1/6}Mn_{1/3}O_2$ ($0 \leqslant x \leqslant 1$), which is consistent with a Mn^{4+} valence state. For fully lithiated $LiNi_{1/3}Fe_{1/6}Co_{1/6}Mn_{1/3}O_2$ ($x = 1$ in Fig. 9a), Ni-t_{2g} states are fully occupied and only one spin direction for the Ni-e_g states is occupied. For Fe-t_{2g} and Fe-e_g only the majority spin states are occupied indicating high-spin Fe^{3+}. The Co-t_{2g} states are fully occupied and Co-e_g states are empty, indicative of Co^{3+}. The Fermi level, E_F is located between the top of occupied Co-t_{2g} bands and unoccupied Fe-t_{2g} states. There is an energy gap of about 0.3 eV between the unoccupied and occupied states. Although it is well know that the calculated energy gaps in GGA are typically smaller than the experimental values, the comparison with the calculated energy gap for $LiNi_{1/3}Co_{1/3}Mn_{1/3}O_2$ (0.7 V)[6] indicates that the electronic conductivity of $LiNi_{1/3}Fe_{1/6}Co_{1/6}Mn_{1/3}O_2$ may be as good, if not better, as $LiNi_{1/3}Co_{1/3}Mn_{1/3}O_2$.

As we applied a supercell with six-formula units in this study, both Ni^{2+}/Ni^{3+} and Ni^{2+}/Ni^{4+} are possible redox reactions. Figure 9a and b show that for a partially delithiated state ($2/3 \leqslant x \leqslant 1$), only the Ni^{2+}/Ni^{3+} redox reaction is observed, which is consistent with the previous studies on $LiNi_{1/2}Mn_{1/2}O_2$ and $LiNi_{1/3}Co_{1/3}Mn_{1/3}O_2$.[6,17,18] At $x = 2/3$ (Fig. 9b), there is an overlap between filled Ni-e_g and Fe-e_g states, indicating very similar redox potentials for Ni and Fe ions. Electrons are simultaneously removed from the Ni-e_g and Fe-e_g bands upon further delithiation as shown in Fig. 9c. It clearly indicates that the Ni^{3+}/Ni^{4+} and Fe^{3+}/Fe^{4+} redox reactions take place simultaneously. Such simultaneous redox reactions of Fe and Ni have been reported in the $Li(Ni,Fe)O_2$ system by

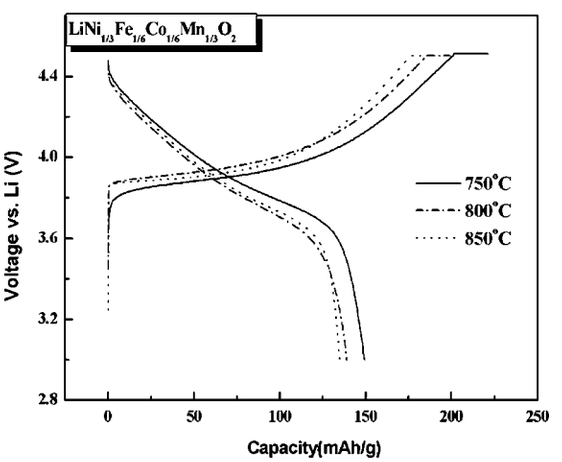

Figure 6. Comparison of first charge-discharge curves of the $LiNi_{1/3}Fe_{1/6}Co_{1/6}Mn_{1/3}O_2$ materials synthesized at 750, 800, and 850°C for 16 h.

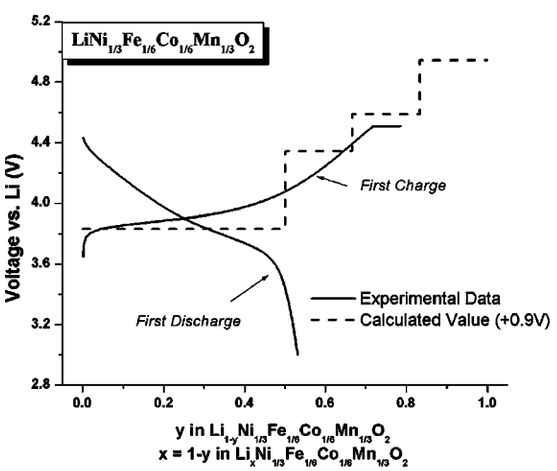

Figure 8. Comparison of experimental potential curve (sample synthesized at 750°C) with the predicted potential curve by first principles calculation.

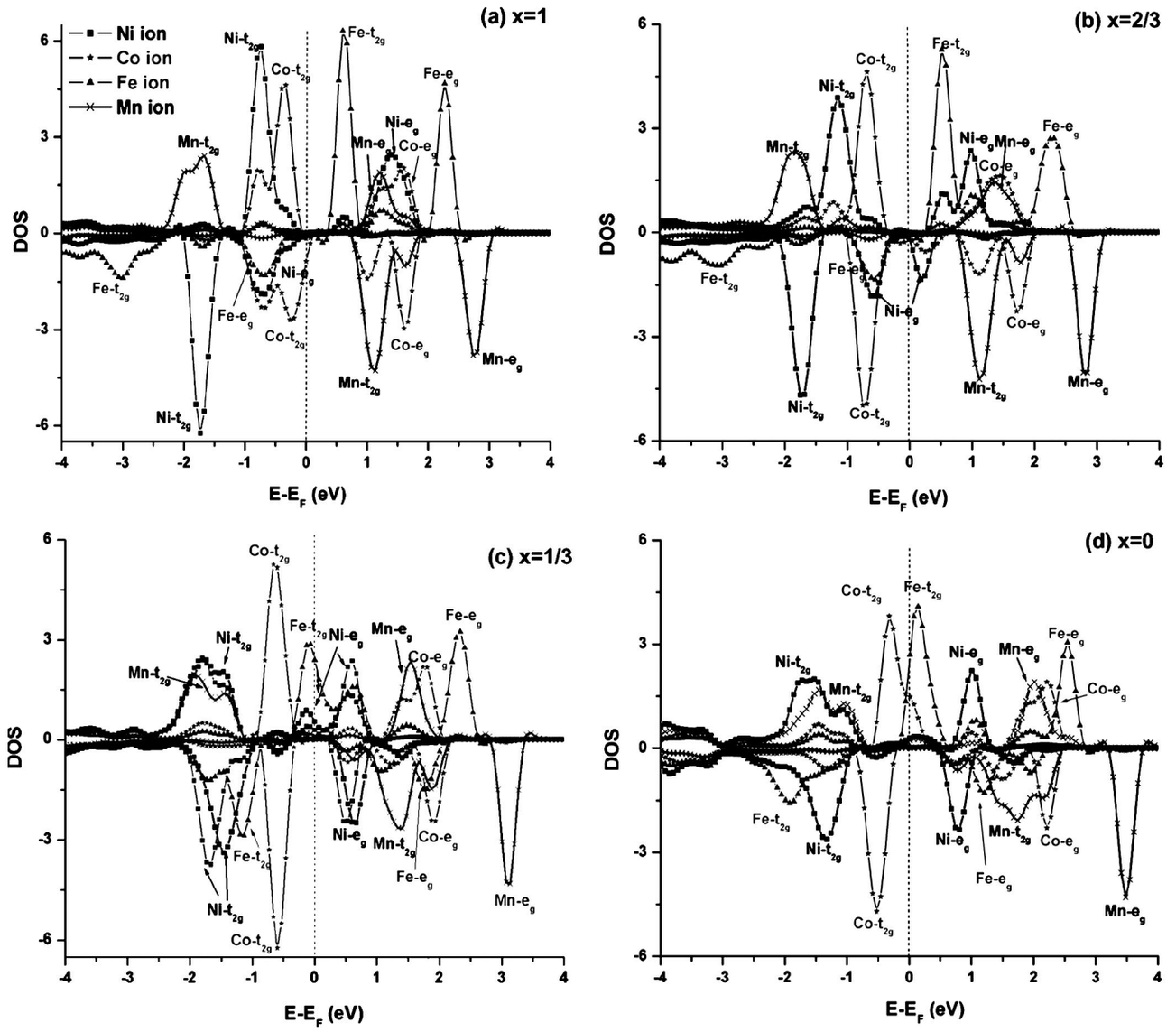

Figure 9. Density of States of $Li_xNi_{1/3}Fe_{1/6}Co_{1/6}Mn_{1/3}O_2$ at (a) $x = 1$, (b) $x = 2/3$, (c) $x = 1/3$, and (d) $x = 0$.

^{57}Fe Mossbauer and extended X-ray absorption fine structure (EXAFS) investigations.[12,14] Furthermore, upon delithiation ($1/3 \leqslant x \leqslant 2/3$), the Fe-$e_g$ states become empty and all four valence electrons partially fill Fe-t_{2g} states indicating low-spin for Fe^{4+}. At $x = 0$, an electron is also pulled from the Co-t_{2g} band (Fig. 9d), which demonstrates that the redox couple Co^{3+}/Co^{4+} is activated at the end of charge.

XPS was applied to corroborate the electronic behavior predicted computationally. *Ex situ* XPS study was carried out to study the valence shifts of Ni, Co, Fe, and Mn in $LiNi_{1/3}Fe_{1/6}Co_{1/6}Mn_{1/3}O_2$ and in partially charged $Li_xNi_{1/3}Co_{1/6}Fe_{1/6}Mn_{1/3}O_2$ ($x \approx 1/2$). The electrodes were charged to 4.4 V. The binding energies of those cations in the as-prepared and partially charged compounds are tabulated in Table I. Indicating by the binding energy shift of the 2p electrons for the transition metal cations from their elemental values,[19] XPS confirms that the valence states of Ni, Fe, Co, and Mn in the as-synthesized $LiNi_{1/3}Fe_{1/6}Co_{1/6}Mn_{1/3}O_2$ are 2+, 3+, 3+, and 4+, respectively. Furthermore, as lithium is removed from the compound, both $Ni^{2+}/Ni^{3+}/Ni^{4+}$ and Fe^{3+}/Fe^{4+} redox couples are activated, revealed by an obvious shift in binding energies of Ni 2p and Fe 2p edges. No obvious shifts in Co and Mn edges were observed. The results are in good agreement with the calculated change of valence states during delithiation.

Lattice parameters and bond lengths.—The calculated lattice parameters a & c at various lithium concentrations are depicted in Fig. 10. The structural parameters of the most stable states were

Table I. XPS binding energy for as-prepared and partially charged materials.

	Ni $2p_{3/2}$/eV	Fe $2p_{3/2}$/eV	Co $2p_{3/2}$/eV	Mn $2p_{3/2}$/eV
$LiNi_{1/3}Fe_{1/6}Co_{1/6}Mn_{1/3}O_2$	854.7 (1.7)	710.9 (3.9)	780.4 (1.4)	842.3 (3.3)
$Li_xNi_{1/3}Fe_{1/6}Co_{1/6}Mn_{1/3}O_2$ $x \approx 1/2$	855.5 (2.5)	711.8 (4.8)	780.4 (1.4)	842.1 (3.1)

Number in the parentheses—shift in binding energy.

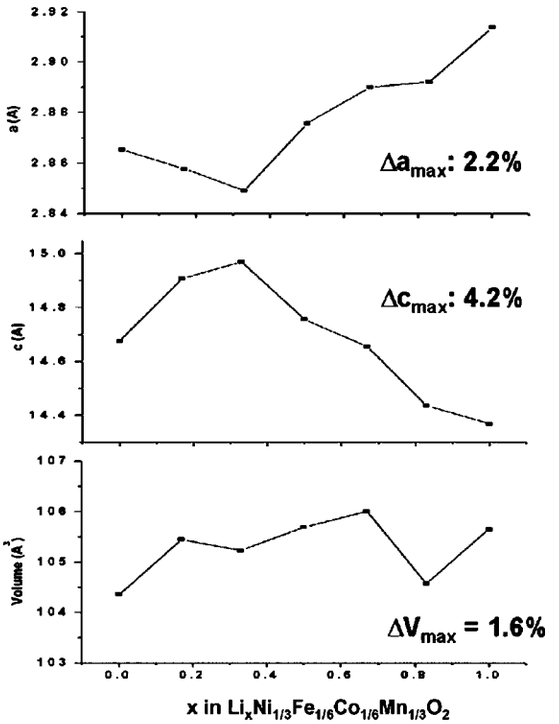

Figure 10. Calculated lattice parameter *a* & *c* and volume at various lithium concentrations.

selected.There is no significant difference in the structural parameters among different lithium-vacancy configurations at the same composition.

The calculated a lattice parameter decreases in the range of $1/3 \leqslant x \leqslant 1$ by approximately 2.2% and increases slightly in the range of $0 \leqslant x \leqslant 1/3$. The lattice parameter c increases by about 4.2% in the range of $1/3 \leqslant x \leqslant 1$ and decreases for $0 \leqslant x \leqslant 1/3$. The maximum change in cell volume is only 1.6%, which implies that effect of stress and strain in the material during the lithiation-delithiation cycle will be very small. In comparison the volume change of $LiCoO_2$ is about 3 to 4 percent.[20]

The average bond distances between the transition metal ions and oxygen ions at different lithium contents are plotted in Fig. 11. The bond distances of Ni-O and Mn-O in fully lithiated $Li_xNi_{1/3}Fe_{1/6}Co_{1/6}Mn_{1/3}O_2$ material ($x = 1$) are [2 × 2.04 2.05 2 × 2.06 2.07] Å, [2.06 2.07 2.08 3 × 2.09] Å, and [1.93 4 × 1.94 1.95] Å, [3 × 1.93 1.94 2 × 1.95] Å, respectively. The bond distance of Ni-O is much longer than that of Mn-O, indicating Ni has oxidation state of 2+ in this material. Fe-O has similar bond distances as Ni-O [2.04 4 × 2.05 2.06] Å, which can be explained by the similar size of Fe^{3+} and Ni^{2+} [Shannon radius].[21] Co-O has the typical bond distance of Co^{3+} in the layered compound.[22]

As lithium is removed, in the range of $2/3 \leqslant x \leqslant 1$, Ni^{2+} is oxidized and the bond distances of Ni-O become shorter. The large spread of bond lengths for Ni-O in his range is due to Jahn-Teller distortion of $Ni^{III}O_6$ octahedron. Note that this also affects the Fe-O and Mn-O bond lengths. Such distortion disappears upon further lithium removal: in the range of $1/3 \leqslant x \leqslant 2/3$, the Fe-O (Fig. 11c) and Ni-O (Fig. 11a and b) bond distances reduce simultaneously, which is in good agreement with the DOS observations in Fig. 9. In addition, in this range ($1/3 \leqslant x \leqslant 2/3$) the decrease in Fe-O bonds distance changes the crystal field splitting between the e_g and t_{2g} bands,[23] which leads to low-spin of Fe^{4+}, as mentioned previously.

Conclusions

Motivated by a series of first principles calculations on $LiNi_{1/3}Co_{1/3}Mn_{1/3}O_2$ with Co or Mn substituted by other metals, $LiNi_{1/3}Fe_{1/6}Co_{1/6}Mn_{1/3}O_2$ was synthesized by a sol-gel method. We

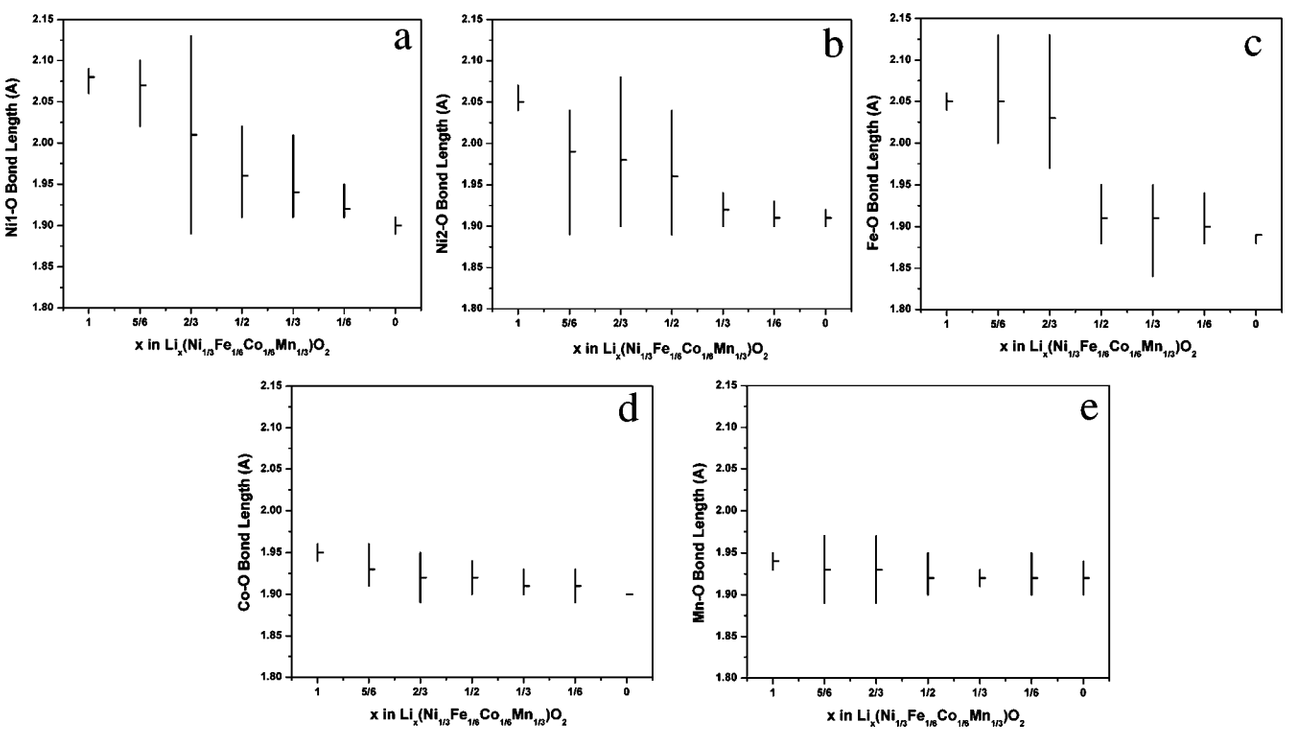

Figure 11. Calculated transition metal—oxygen bond (TM-O) distances of $Li_xNi_{1/3}Fe_{1/6}Co_{1/6}Mn_{1/3}O_2 (0 \leqslant x \leqslant 1)$.

predicted and confirmed that Fe substitution would lead to a lower potential at the end of charge. Both XPS and first principles electronic structure computations indicate that Ni and Fe are simultaneously oxidized in this material. Computations further indicate that Co will only be oxidized at the very end of charge. The $LiNi_{1/3}Fe_{1/6}Co_{1/6}Mn_{1/3}O_2$ compound synthesized at 750°C shows reversible capacity of 150 mAh/g with reasonably good capacity retention. In this work, we have demonstrated that an integrated approach of computation and experiment has produced a new electrode material with very few iteration steps in the material design cycle. We believe that such direct integration of ab-initio methods with experimental research holds promise for significantly shortening the development cycle of materials.

Acknowledgments

This work was supported in part by the MRSEC Program of the National Science Foundation under award number DMR 02-13282 and by the Singapore-MIT Alliance. We thank NPACI for the computing resources.

MIT assisted in meeting the publication costs of this article.

References

1. T. Ohzuku and Y. Makimura, *Chem. Lett.*, **2001**, 744.
2. Z. H. Lu, D. D. MacNeil, and J. R. Dahn, *Electrochem. Solid-State Lett.*, **4**, A200 (2001).
3. Z. H. Lu, D. D. MacNeil, and J. R. Dahn, *Electrochem. Solid-State Lett.*, **4**, A191 (2001).
4. J. Reed, G. Ceder, and A. Van Der Ven, *Electrochem. Solid-State Lett.*, **4**, A78 (2001).
5. N. Yabuuchi and T. Ohzuku, *J. Power Sources*, **119**, 171 (2003).
6. B. J. Hwang, Y. W. Tsai, D. Carlier, and G. Ceder, *Chem. Mater.*, **15**, 3676 (2003).
7. K. M. Shaju, G. V. Subba Rao, and B. V. R. Chowdari, *Electrochim. Acta*, **48**, 145 (2002).
8. A. Van der Ven, M. K. Aydinol, G. Ceder, G. Kresse, and J. Hafner, *Phys. Rev. B*, **58**, 2975 (1998).
9. C. Wolverton and A. Zunger, *J. Electrochem. Soc.*, **145**, 2424 (1998).
10. G. Ceder, Y. M. Chiang, D. R. Sadoway, M. K. Aydinol, Y. I. Jang, and B. Huang, *Nature (London)*, **392**, 694 (1998).
11. S. K. Mishra and G. Ceder, *Phys. Rev. B, Condens. Matter*, **59**, 6120 (1999).
12. A. Demourgues, in *Lithium Batterie Discussion*, Arcachon (2001).
13. C. Delmas, M. Menetrier, L. Croguennec, I. Saadoune, A. Rougier, C. Pouillerie, G. Prado, M. Grune, and L. Fournes, *Electrochim. Acta*, **45**, 243 (1999).
14. G. Prado, L. Fournès, and C. Delmas, *J. Solid State Chem.*, **159**, 103 (2001).
15. T. A. Hewston and B. L. Chamberland, *J. Phys. Chem. Solids*, **48**, 97 (1987).
16. M. K. Aydinol, A. F. Kohan, G. Ceder, K. Cho, and J. Joannopoulos, *Phys. Rev. B*, **56**, 1354 (1997).
17. Y. Arachi, H. Kobayashi, S. Emura, Y. Nakata, M. Tanaka, and T. Asai, *Chem. Lett.*, **32**, 60 (2003).
18. J. Reed and G. Ceder, *Electrochem. Solid-State Lett.*, **5**, A145 (2002).
19. www.srdata.nist.gov/xps
20. T. Ohzuku and A. Ueda, *J. Electrochem. Soc.*, **141**, 2972 (1994).
21. R. D. Shannon, *Acta Crystallogr.*, **32**, 751 (1976).
22. Y. Koyama, I. Tanaka, H. Adachi, Y. Makimura, and T. Ohzuku, *J. Power Sources*, **119-121**, 644 (2003).
23. B. N. Figgis and M. A. Hitchman, *Ligand Field Theory and its Applications*, Wiley-VCH, New York (2000).